JOURNAL OF GUIDANCE, CONTROL, AND DYNAMICS
Vol. 27, No. 3, May–June 2004

Resonant Motion of a Spin-Stabilized Thrusting Spacecraft

Ja-Young Kang*
Hankuk Aviation University, Gyeonggi-do 412-791, Republic of Korea
and
John E. Cochran Jr.†
Auburn University, Auburn, Alabama 36849-5338

The attitude instability of a spin-stabilized, thrusting upper stage spacecraft is investigated based on a two-body model consisting of a symmetric main body, representing the spacecraft, and a spherical pendulum, representing the liquefied slag pool entrapped in the aft section of the rocket motor. Exact time-varying nonlinear equations are derived and used to eliminate the drawbacks of conventional linear models. To study the stability of the spacecraft's attitude motion, both the spacecraft and pendulum are assumed to be in states of steady spin about the symmetry axis of the spacecraft and the coupled time-varying nonlinear equation of the pendulum is simplified. A quasi-stationary solution to that equation and approximate resonance conditions are determined in terms of the system parameters. The analysis shows that the pendulum is subject to a combination of parametric and external-type excitation by the main body and that energy from the excited pendulum is fed into the main body to develop the coning instability. When one of the resonance conditions and real flight data are used in the original time-varying nonlinear equations, the results match well with the observed motion before and after motor burnout of typical spin-stabilized upper stages. Some numerical examples are presented to explain the mechanism of the coning angle growth and how disturbance moments are generated.

Nomenclature

a	=	transverse component of the system angular momentum
$\boldsymbol{a}_C$	=	acceleration of the center of mass, C
C_1, C	=	centers of masses of the main body and the system
$\boldsymbol{E}$	=	3×3 identity matrix
$\boldsymbol{F}$	=	thrust vector $(0\ \ 0\ \ F_3)^T$ along the symmetry axis passing through C_1
$\boldsymbol{H}, \boldsymbol{h}$	=	angular momenta of the system and the pendulum
$\boldsymbol{I}$	=	centroidal inertia dyadic of the spacecraft body
m_1, m_2	=	masses of spacecraft main body and pendulum bob
O	=	pivot point of the pendulum
r	=	length of massless rod connecting the pendulum bob
$\boldsymbol{r}, \boldsymbol{r}_o, \boldsymbol{r}_p$	=	position vectors from O to m_2, C_1 to O, and C_1 to m_2
$\boldsymbol{r}_1, \boldsymbol{r}_2$	=	position vectors from C to C_1 and m_2, respectively
$\boldsymbol{T}$	=	torque generated by deviation of C from the line of thrust vector $\boldsymbol{F}$
$\boldsymbol{T}_o$	=	frictional torque about O
$\boldsymbol{u}_r, \boldsymbol{u}_p$	=	unit vectors of $\boldsymbol{r}$ and $\boldsymbol{r}_p$, respectively
$\boldsymbol{v}_C, \boldsymbol{v}_1, \boldsymbol{v}_2$	=	velocities of C, C_1 and m_2
$x_1y_1z_1$	=	body-fixed frame having its origin at C_1
β, β_e	=	pendulum near-resonant and excitation frequencies
ε	=	nondimensional small parameter
θ, ψ	=	radial and circumferential coordinates for the pendulum
θ_s, ϑ	=	stationary point of θ and variation from that point
μ	=	ratio of m_2 to the total mass, $m_1 + m_2$
$\boldsymbol{\xi}$	=	pendulum generalized coordinates, i.e. $(\theta, \psi)^T$
σ	=	parameter describing the nearness of the excitation frequency to the system frequency
τ	=	scaled time
Φ	=	angle of rotation of the main body
$\boldsymbol{\omega}$	=	angular velocity of the centroidal coordinate system $x_1y_1z_1$

Subscripts

e	=	excitation
o	=	pendulum pivot point
p	=	pendulum
r	=	length of the pendulum
s	=	stationary

Superscript

$\times$	=	skew symmetric matrix used to form components of cross products of vectors

Received 11 October 2002; revision received 20 September 2003; accepted for publication 20 September 2003.

*Assistant Professor, Department of Aeronautical Science and Flight Operation, Goyang City. Member AIAA.

†Professor and Head, Department of Aerospace Engineering. Associate Fellow AIAA.

I. Introduction

USUALLY, nutation of a spinning spacecraft is caused by a single asymmetric impulse due to, for example, separation spring imbalance, rocket motor tailoff, motor side forces, thrust vector misalignment, or principal axis misalignment. However, the nutation instability of certain upper stage spacecraft, known as the Payload Assist Module, Delta Class (PAM-D) coning anomaly, has not been explained by such conventional disturbances. What has been determined is that the source of the instability is related in some way to the operation of the rocket motor.

Based on analyses of flight data (Fig. 1), several mechanisms have been proposed to account for the anomalous attitude motion of spacecraft of interest. The jet gain theory, one of the principal theories advanced to explain the anomalous motion, was developed by Flandro,[1] Flandro et al.,[2] and Roach et al.[3]

This theory proposes that the conservation of angular momentum creates a vortex as the propellant surface gases approach the centerline of a spinning motor. The circumferential flow velocity induced by the vortex velocity field is greatly intensified as the vortex core is stretched through the nozzle throat. Small wobbling of the spacecraft induces an asymmetrical pressure distribution within the combustion chamber that is related to the classical inertial wave phenomenon. The fluctuating velocity field associated with this wave

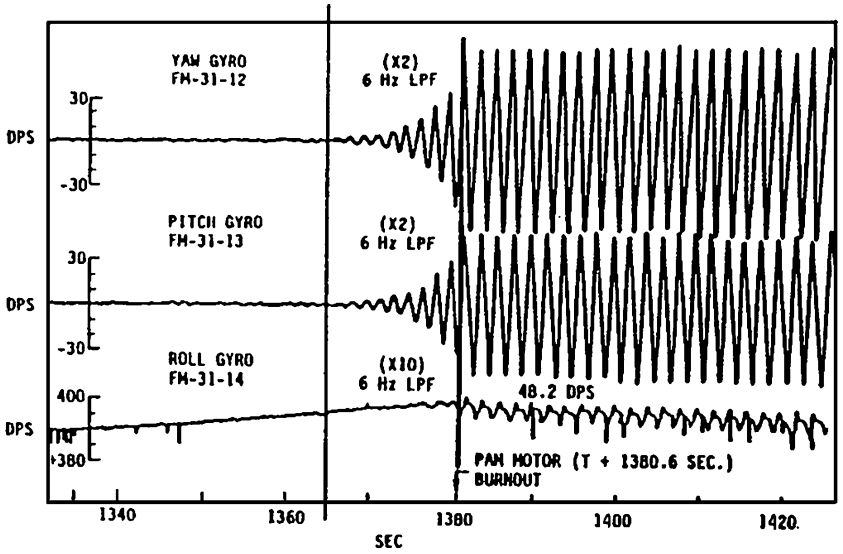

Fig. 1 Flight data telemetered from RCA-C′ (Ref. 11).

interacts strongly with the vortex core causing an undulating vortex filament that orbits the spin axis as it leaves the chamber and enters the nozzle.

The second major candidate is the slag pool theory,[4–9] which is based partially on empirical evidence that states that byproducts of combustion can collect within the aft portion of the spinning solid rocket motor around the submerged nozzle during thrusting of the vehicle. Usually, aluminum is added to solid propellant to improve performance and to suppress high-frequency combustion instability.[4] This pool of accumulated slag may grow with time and can serve as an energy storage and/or dissipation source that interacts with the spacecraft motion. However, modeling the slag is not a simple matter and is perhaps the most important part in the analysis. Boraas[7] developed an analytical procedure for calculating specific quantities relating to the deposition and pooling of slag in a spinning solid rocket motor. He explained that most of slag deposition takes place near the end of the motor burn. Haloulakas[8] also developed a slag mass accumulation model and computed the quantities of slag mass as a function of spin rate for some spin-stabilized solid rocket motors. He showed that, at high spin rates, the effects of the axial accelerations are less significant. Frederick et al.[9] experimentally determined the slag accumulation characteristics inside a strategic-sized solid rocket motor. In his model, he observed that slag sloshed at low frequencies. This makes it possible to use the hypothesis that the sloshing motion of the slag is amplified by interaction with the axial thrust and drives the coning growth of the spacecraft.

Various equivalent mechanical models have been proposed to describe the motion of liquid in its moving container. Several researchers[10–12] have investigated the stability of a spacecraft's attitude motion by adopting equivalent pendulum models to represent the effects of fluid slosh. Also, some research work[13–16] identifying the accumulated slag as a cause of the observed coning anomaly of the PAM upper stage spacecraft has been done. This approach is a somewhat idealized one, but is helpful in gaining an understanding of the uncertain complex slag physics. Mingori and Yam[17] developed linear stability conditions for a spacecraft consisting of an axisymmetric rigid body and a planar pendulum to represent the sloshing mass. In their model, the pendulum mass is attached to its pivot by a spring and is free to rotate about the symmetry axis of the spacecraft. Assuming that the spacecraft is in a state of steady spin about its symmetry axis, they obtained linear equations and showed the possibility for unstable coning growth if the thrust magnitude is sufficiently large and the moving mass is aft of the system mass center. Yam et al.[18] also examined how the stability regions are modified when the dissipative forces are added to the previous model.

Cochran and Kang[13] have obtained some significant results for the attitude motion of the spinning upper stage using an asymmetric main body plus a spherical pendulum model. First, they derived the exact time-varying nonlinear equations. Then, by treating the motion of the pendulum as a perturbation of the motion of the spacecraft as a whole, they obtained approximate nonlinear equations in terms of angular momentum variables. Some numerical experiments were conducted for three cases: 1) no viscosity in the model, 2) viscous effects models by a linear damper, and 3) variable viscous interactions of the pendulum motion with main body. This experiment was performed using the real flight parameters and taking into account the dynamics of slag accumulation. Results of the numerical experiments showed that coning instability occurs during the thrusting phase and that the coning motion stabilizes after the motor burnout. Or[14] also carried out a linear analysis of the stability of a spinning, thrusting spacecraft. To model the liquid pool, he used two types of pendulum models, one being a spherical pendulum model and the other consisting of two orthogonal plane pendulums. His results showed that both models will produce unstable motion if tuned pendulum conditions are used. Or and Challoner[15] also analyzed the effect of sloshing with a linearized hydrodynamic coupled finite element method. Meyer[16] analyzed the instability of spin-stabilized spacecraft based on a hydrodynamic model of liquid slag trapped in the motor. The analysis is closely related to the classic shallow fluid or tidal theory.

By investigating the effect of the baffle on the fluid propellant motion of the spacecraft, Hung[19] suggested a method of passive control by using a baffle to damp the amplitude of slosh wave excitation and lower the angular momentum and fluid moment fluctuation. Cho et al.[20] developed a mathematical model of the spacecraft using a pendulum to represent the fuel slosh and a nonlinear feedback controller that can be modified to control actively the motion of the spacecraft subject to the slag slosh excitation.

The objectives of this study are to present a derivation of the mathematical model, to identify conditions for nonlinear resonance, and to use the model to show how nonlinear resonance causes coning instability that is similar to the coning instabilities observed in the attitude motions of PAM-D type spacecraft, as well as to show the appropriateness of the model.

This paper presents an analysis of the dynamics of a spinning upper stage spacecraft based on a two-body model consisting of a symmetric main body, representing the spacecraft, and a spherical pendulum, representing the liquefied slag pool entrapped in the aft section of the rocket motor. Exact time-varying nonlinear equations are derived and used to eliminate the drawback of the conventional linear models. To study the stability of the spacecraft's attitude motion, both the spacecraft and pendulum are assumed to be in states of steady spin about the symmetry axis of the spacecraft, and the coupled time-varying nonlinear equation of the pendulum is simplified. A quasi-stationary solution to that equation and approximate resonance conditions are determined in terms of the system

parameters. Numerical results are presented to illustrate the effects of near-resonant conditions on the attitude motion of the spacecraft.

II. Physical and Mathematical Models

Figure 2 shows a two-body model consisting of a rigid body, representing the spacecraft main body, and a point-mass spherical pendulum, representing a liquid pool.[13] The rigid body has mass m_1, centroidal, principal moments of inertia $I_1 \geq I_2 > I_3$ about the axes x_1, y_1, and z_1, respectively, and center of mass C_1. The pendulum consists of a point mass m_2 attached to a rigid, massless rod, which in turn is attached at a point O to the body m_1. Its motion with respect to the body m_1, is defined by the angles θ and ψ.

Equations of motion may be derived for the system of two bodies by using various methods. The method used is the Newton–Euler method, and the equations for θ and ψ are obtained by finding two orthogonal components that are perpendicular to the vector $\boldsymbol{r}$, which is constrained in length.

The $x_1y_1z_1$ axes are fixed in the reference body with the origin at C_1 and rotate with that body at an angular velocity $\boldsymbol{\omega}$. If we define a position vector from C to m_i as $\boldsymbol{r}_i$ and velocity vector of m_i as $\boldsymbol{v}_i$, equations governing the motion for the system about its center of mass may be derived by first writing the angular momentum of the system about C in the form

$$\boldsymbol{H} = \boldsymbol{I} \cdot \boldsymbol{\omega} + \boldsymbol{m}_1\boldsymbol{r}_1 \times \boldsymbol{v}_1 + \boldsymbol{m}_2\boldsymbol{r}_2 \times \boldsymbol{v}_2 \tag{1}$$

Because

$$\boldsymbol{r}_1 = -[m_2/(m_1+m_2)](\boldsymbol{r}_o + \boldsymbol{r}) = -\mu\boldsymbol{r}_p \tag{2}$$

$$\boldsymbol{r}_2 = (1-\mu)\boldsymbol{r}_p \tag{3}$$

$$\boldsymbol{v}_1 = \boldsymbol{v}_C - \mu(\boldsymbol{\omega} \times \boldsymbol{r}_p + \dot{\boldsymbol{r}}_p) \tag{4}$$

$$\boldsymbol{v}_2 = \boldsymbol{v}_C + (1-\mu)(\boldsymbol{\omega} \times \boldsymbol{r}_p + \dot{\boldsymbol{r}}_p) \tag{5}$$

Equation (1) becomes

$$\boldsymbol{H} = \boldsymbol{I} \cdot \boldsymbol{\omega} + \mu m_1 \boldsymbol{r}_p \times (\boldsymbol{\omega} \times \boldsymbol{r}_p + \dot{\boldsymbol{r}}_p) \tag{6}$$

where $\boldsymbol{r}_p = \boldsymbol{r}_o + \boldsymbol{r}$ and $\dot{\boldsymbol{r}}_p$ is the time rate of change of $\boldsymbol{r}_p$ due to motion of the pendulum relative to m_1. By writing Eq. (6) in matrix form, we have

$$\boldsymbol{H} = \boldsymbol{J} \cdot \boldsymbol{\omega} + \boldsymbol{h} \tag{7}$$

where $\boldsymbol{J} = \boldsymbol{I} - \mu m_1 \boldsymbol{r}_p^{\times}\boldsymbol{r}_p^{\times}$, $\boldsymbol{h} = \mu m_1 \boldsymbol{r}_p^{\times}\dot{\boldsymbol{r}}$, and $\boldsymbol{r} = r(-\sin\theta\sin\psi \quad \sin\theta\cos\psi \quad -\cos\theta)^T$. Here, the $\times$ superscript over $\boldsymbol{r}_p$ denotes the skew-symmetric matrix used to form components of cross products of vectors.[21] The time derivative of the vector $\boldsymbol{H}$ and Eq. (7) may be used to get the matrix equations,

$$\dot{\boldsymbol{H}} = \boldsymbol{H}^{\times}\boldsymbol{J}^{-1}(\boldsymbol{H} - \boldsymbol{h}) + \boldsymbol{T} \tag{8}$$

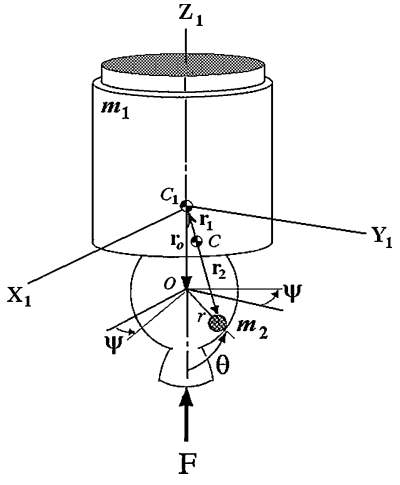

Fig. 2 Two-body spacecraft model.

where $\boldsymbol{T}$ is an external torque about the C. To model $\boldsymbol{T}$, we assume that the thrust vector $\boldsymbol{F}$ passes through the point C_1. Then,

$$\boldsymbol{T} = -\mu\boldsymbol{r}_p^{\times}\boldsymbol{F} \tag{9}$$

An equation for the relative motion of the pendulum is more difficult to find. One way to obtain a suitable equation is to write the absolute acceleration of m_2, equate it to the force on m_2 and cross $\boldsymbol{r}$ into both sides of the resulting equation. Let $\boldsymbol{a}_C$ be the acceleration of the center of system mass (m_1+m_2). Then, the absolute acceleration of m_2 can be expressed as

$$\boldsymbol{a}_p = \boldsymbol{a}_C + \frac{\mathrm{D}^2\boldsymbol{r}_2}{\mathrm{D}t^2} = \boldsymbol{a}_C + (1-\mu)\frac{\mathrm{D}^2\boldsymbol{r}_p}{\mathrm{D}t^2}$$

$$= \boldsymbol{a}_C + (1-\mu)\left[\ddot{\boldsymbol{r}} + \dot{\boldsymbol{\omega}}^{\times}\boldsymbol{r}_p + 2\boldsymbol{\omega}^{\times}\dot{\boldsymbol{r}} + \boldsymbol{\omega}^{\times}\left(\boldsymbol{\omega}^{\times}\boldsymbol{r}_p\right)\right] \tag{10}$$

where $\boldsymbol{r}_2$ is a position vector from C to the pendulum bob and $\mathrm{D}(\cdot)/\mathrm{D}t$ is the time derivative of a vector as seen from a nonrotating reference frame. Therefore, the moment equation about the pendulum pivot point O becomes

$$\boldsymbol{T}_o = m_2\boldsymbol{r}^{\times}\boldsymbol{a}_C + \mu m_1\boldsymbol{r}^{\times}\left(\ddot{\boldsymbol{r}} - \boldsymbol{r}_p^{\times}\dot{\boldsymbol{\omega}} + 2\boldsymbol{\omega}^{\times}\dot{\boldsymbol{r}} - \boldsymbol{\omega}^{\times}\boldsymbol{r}_p^{\times}\boldsymbol{\omega}\right) \tag{11}$$

where $\boldsymbol{T}_o$ is a torque about the pivot point O. When $\boldsymbol{a}_C$ is replaced by $\boldsymbol{F}/(m_1+m_2)$, Eq. (11) becomes

$$\boldsymbol{T}_o = \mu m_1 r^2 \boldsymbol{u}_r^{\times}\left(\ddot{\boldsymbol{u}}_r - \boldsymbol{u}_p^{\times}\dot{\boldsymbol{\omega}} + 2\boldsymbol{\omega}^{\times}\dot{\boldsymbol{u}}_r - \boldsymbol{\omega}^{\times}\boldsymbol{u}_p^{\times}\boldsymbol{\omega} + \boldsymbol{F}/m_1 r\right) \tag{12}$$

Because $\dot{\boldsymbol{\omega}}$ appears in Eq. (12) instead of $\dot{\boldsymbol{H}}$, there is added complication in solving the equation for $\ddot{\theta}$ and $\ddot{\psi}$. However, necessary substitutions may be carried out fairly easily in a digital computer program. If $\dot{\boldsymbol{\omega}}$ and $\boldsymbol{\omega}$ are eliminated from Eq. (12), the resulting equation becomes

$$\boldsymbol{T}_o = \mu m_1 r^2 \boldsymbol{u}_r^{\times}\Big(\left(\boldsymbol{E} + \mu m_1 r^2 \boldsymbol{u}_p^{\times}\boldsymbol{J}^{-1}\boldsymbol{u}_p^{\times}\right)\ddot{\boldsymbol{u}}_r - \Big\{\boldsymbol{u}_p^{\times}\boldsymbol{J}^{-1}\boldsymbol{H}^{\times}$$

$$+ \left(2\boldsymbol{E} + \mu m_1 r^2 \boldsymbol{u}_p^{\times}\boldsymbol{J}^{-1}\boldsymbol{u}_p^{\times}\right)\dot{\boldsymbol{u}}_r^{\times} + [\boldsymbol{J}^{-1}(\boldsymbol{H}-\boldsymbol{h})]^{\times}\boldsymbol{u}_p^{\times}\Big\}\boldsymbol{J}^{-1}(\boldsymbol{H}-\boldsymbol{h})$$

$$+ \left[\mu r \boldsymbol{u}_p^{\times}\boldsymbol{J}^{-1}\boldsymbol{u}_p^{\times} + (1/m_1 r)\boldsymbol{E}\right]\boldsymbol{F}\Big) \tag{13}$$

Then, we may find the necessary equations by using the matrix

$$\boldsymbol{B} = \begin{bmatrix} \cos\psi & \sin\psi & 0 \\ -\sin\psi & \cos\psi & 0 \\ 0 & 0 & 0 \end{bmatrix} \tag{14}$$

The first row of $\boldsymbol{B}$ is a unit vector perpendicular to the plane in which θ is measured. The second row is a unit vector orthogonal to the first row. Let $\boldsymbol{\xi} = [\theta \quad \psi]^T$. Then, because

$$\dot{\boldsymbol{u}}_r = \begin{bmatrix} -\cos\theta\sin\psi & -\sin\theta\cos\psi \\ \cos\theta\cos\psi & -\sin\theta\sin\psi \\ \sin\theta & 0 \end{bmatrix}\begin{pmatrix} \dot{\theta} \\ \dot{\psi} \end{pmatrix} \tag{15}$$

the equation of motion for the pendulum can be written as

$$\boldsymbol{B}\boldsymbol{A}_1\boldsymbol{A}_2\ddot{\boldsymbol{\xi}} = \boldsymbol{B}(\boldsymbol{G} - \boldsymbol{A}_1\dot{\boldsymbol{A}}_2\dot{\boldsymbol{\xi}}) \tag{16}$$

where

$$\boldsymbol{A}_1 = \boldsymbol{u}_r^{\times}\left(\boldsymbol{E} + \mu m_1 r^2 \boldsymbol{u}_p^{\times}\boldsymbol{J}^{-1}\boldsymbol{u}_p^{\times}\right) \tag{17}$$

$$\boldsymbol{A}_2 = \begin{bmatrix} -\cos\theta\sin\psi & -\sin\theta\cos\psi \\ \cos\theta\cos\psi & -\sin\theta\sin\psi \\ \sin\theta & 0 \end{bmatrix} \tag{18}$$

$$\boldsymbol{G} = \boldsymbol{u}_r^{\times}\Big\{\boldsymbol{u}_p^{\times}\boldsymbol{J}^{-1}\boldsymbol{H}^{\times} + \left(2\boldsymbol{E} + \mu m_1 r^2 \boldsymbol{u}_p^{\times}\boldsymbol{J}^{-1}\boldsymbol{u}_p^{\times}\right)(\boldsymbol{A}_2\dot{\boldsymbol{\xi}})^{\times}$$

$$+ [\boldsymbol{J}^{-1}(\boldsymbol{H}-\boldsymbol{h})]^{\times}\boldsymbol{u}_p^{\times}\Big\}\boldsymbol{J}^{-1}(\boldsymbol{H}-\boldsymbol{h})$$

$$- \boldsymbol{u}_r^{\times}\left(\mu r \boldsymbol{u}_p^{\times}\boldsymbol{J}^{-1}\boldsymbol{u}_p^{\times} + \boldsymbol{E}/m_1 r\right)\boldsymbol{F} + \boldsymbol{T}_o\big/\mu m_1 r^2 \tag{19}$$

Equations (8) and (16), along with suitable kinematic equations for the Euler angles Θ_1, Θ_2, and Θ_3, constitute a mathematical model of the systems, but they do not provide any insight into the possibility of resonances.

III. Resonance Analysis

A. Stationary Solutions of the Pendulum Motion

Because the pendulum motion is suspected as the main source driving the anomalous attitude motion, we are encouraged to investigate the instability of the system by examining the stability of the pendulum motion by either a numerical method or an analytical method. In the case of using the numerical method, one may first find a stationary relative orientation of the pendulum and then conduct numerical experiments for the stability of the system using full nonlinear equations at the stationary point or in its vicinity. Using the analytical method, one may find the conditions of the resonant motion in terms of parameters and then obtain near-resonant solutions.

The motion of the pendulum during motor burn is balanced by the axial acceleration due to thrust, centrifugal force due to spin of the main body, and a normal force along the pendulum arm, and thus, the pendulum may have certain dynamic equilibrium points. However, because the equation set consists of highly coupled, nonstationary and time-varying, nonlinear equations, neither linear solutions nor nonlinear solutions for the given full equations can be obtained directly without further assumptions. Such difficulties arise from the relatively complex nature of the motion of the spherical pendulum coupled to the dynamics of the spinning, thrusting main body. If we makes the pendulum equations somewhat simpler and find solutions to them, the entire problem may be solved. To do this, further assumptions are made such that both the spacecraft and pendulum are in states of quasi-steady spin about the symmetry axis of the spacecraft. For convenience, we introduce new variables a and Φ (Ref. 22) and w such that

$$H_1 = a\sin\Phi, \qquad H_2 = a\cos\Phi \tag{20}$$

$$w = \psi + \Phi \tag{21}$$

where a is a transverse angular momentum component and rotates at a relative spin rate[21]

$$\dot{\Phi} = (1 - I_3/I_1)\, H_3/I_3 + \mathcal{O}(\varepsilon) \tag{22}$$

with respect to the body. With the assumption that the viscosity effect is negligible during motor operation,[16] that is $\boldsymbol{T}_o \approx 0$, substituting Eqs. (20) and (21) into Eqs. (8) and (13) and selecting the dominant terms yield the following approximate equation for θ:

$$\begin{aligned}\ddot{\theta} = \Big\{\Big[P^2 + \mu(F_3 r_o/I_1) - \left(a^2/2I_1^2\right)(1+\cos 2w)\Big]\cos\theta \\ - (F_3/m_1 r)\left[1 - \mu\left(m_1 r^2/I_1\right)\right] - a^2 r_o/I_1^2 r\Big\}\sin\theta \\ + \left(aH_3/I_1^2\right)[1 + (r_o/r)\cos\theta]\cos w - (2aP/I_1)\sin^2\theta\cos w\end{aligned} \tag{23}$$

where $P = (\dot{\psi} + H_3/I_3)$.

At the beginning of thrusting or in a nonresonance case, a is relatively small so that the following stationary solution of θ may be obtained:

$$\begin{aligned}\theta_s = \cos^{-1}\left(F_3/m_1 r P^2\right)\Big\{1 - \varepsilon\Big[1 + \left(F_3/m_1 r P^2\right)(r_o/r)\Big] \\ + \varepsilon^2\left(F_3/m_1 r P^2\right)(r_o/r)\cdots\Big\}\end{aligned} \tag{24}$$

where $\varepsilon = \mu m_1 r^2/I_1$. As seen in Eq. (24), the equilibrium points of θ are determined mainly by axial and centrifugal accelerations. Because the rocket-thrusting spacecraft is a typical time-varying, nonstationary, nonlinear system, a pendulum attached to such a system may not stay at one equilibrium point all of the times and some stationary points turn into unstable ones with the elapse of time. Therefore, using the term quasi-stationary point (QSP) is better than using the term stationary point.

Table 1 Basic data for the system

Parameters	At $t=0$	At $t=30$	Unit
F_3	16,000	16,000	lb_f
m_1	4,300	2,700	lb_m
m_2	10	30	lb_m
I_1, I_2	1,350	700	slug · ft^2
I_3	460	330	slug · ft^2
r_0	3.4	3.4	ft
r	2	2	ft
a	20	varied	slug · ft^2/s
ω_3	52.4	varied	rpm
ψ	arbitrary	varied	deg
Φ	arbitrary	varied	deg

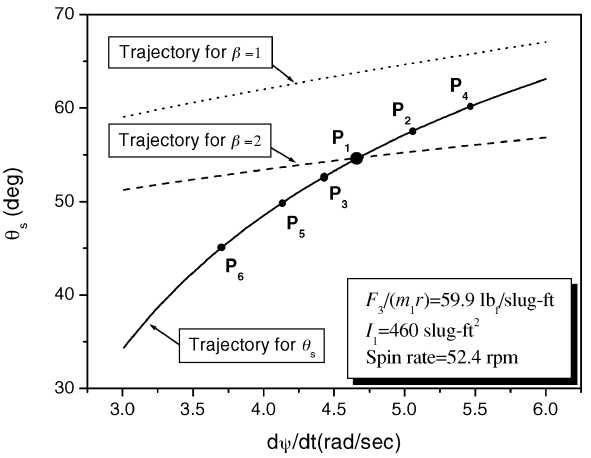

Fig. 3 Quasi-stationary solutions for θ.

Figure 3 shows θ_s vs $\dot{\psi}$ when the data (at $t=0$) given in Table 1 were used. Because the pendulum is supposed to rotate in the same direction as the spacecraft, θ_s is evaluated using only the positive values of $\dot{\psi}$. As expected, the QSP of the pendulum has a tendency to move toward $\pi/2$ as $\dot{\psi}$ increases.

B. Resonance Conditions

If we introduce a term ϑ and expand Eq. (23) about θ_s, a new equation for the pendulum motion at the QSP that includes higher-order terms (HOT) in ϑ is obtained as

$$\begin{aligned}\ddot{\vartheta} &\approx -\left(\frac{F_3}{m_1 r}\cos\theta_s - P^2\cos 2\theta_s + B_1 a\cos w\right)\vartheta + B_2 a\cos w \\ &\quad + \text{HOT} = -\omega_0^2\left(1 + \frac{B_1}{\omega_0^2}a\cos w\right)\vartheta + B_2 a\cos w + \text{HOT}\end{aligned} \tag{25}$$

$$B_1 = \frac{H_3 r_o\sin\theta_s}{I_1^2 r} + \frac{2P\sin 2\theta_s}{I_1}$$

$$B_2 = \frac{H_3 r_o\cos\theta_s}{I_1^2 r} + \frac{P(\cos 2\theta_s - 1)}{I_1} + \frac{H_3}{I_1^2}$$

$$\omega_0^2 = P^2\sin^2\theta_s \tag{26}$$

In a nonresonance case, $B_1 a$ and $B_2 a$ are much smaller than a. As can be observed from Eq. (25), the pendulum is subject to parametric and external excitations. The external excitation is not truly external to the system, but it can be so considered as far as the pendulum is concerned. If the motions are not small, the effect of nonlinearity on stability must be considered. In this paper, motion of the pendulum with respect to the QSP is assumed small so that the HOT in ϑ are dropped from the equation.

For convenience, Eq. (25) can be rewritten in a form similar to Mathieu's equation with forcing functions. To this end, let

$$w = \Omega t + w_0, \qquad t = \left(\frac{2}{\Omega}\right)\tau, \qquad \delta = \frac{4\omega_0^2}{\Omega^2}$$

$$\alpha_1 = \frac{2B_1 a \cos w_0}{\left(m_1 \mu r^2 \Omega^2\right)}, \qquad \alpha_2 = -\frac{2B_1 a \sin w_0}{\left(m_1 \mu r^2 \Omega^2\right)}$$

$$k_1 = \frac{4B_2 a \cos w_0}{\left(m_1 \mu r^2 \Omega^2\right)}, \qquad k_2 = -\frac{4B_2 a \sin w_0}{\left(m_1 \mu r^2 \Omega^2\right)} \tag{27}$$

Then, Eq. (25) can be written in the form

$$\vartheta'' + (\delta + 2\varepsilon\alpha_1 \cos 2\tau + 2\varepsilon\alpha_2 \sin 2\tau)\vartheta = \varepsilon(k_1 \cos 2\tau + k_2 \sin 2\tau) \tag{28}$$

where the double prime denotes $\mathrm{d}^2(\cdot)/\mathrm{d}\tau^2$. To find the resonance conditions for Eq. (28), one may employ the method of multiple scales[23] defined by

$$T_n = \varepsilon^n \tau \qquad \text{for} \qquad n = 0, 1, 2, \ldots \tag{29}$$

Then, the solution of Eq. (28) can be represented by an expansion having the form

$$\vartheta(\tau; \varepsilon) = \vartheta_0(T_0, T_1, T_2, \ldots) + \varepsilon\vartheta_1(T_0, T_1, T_2, \ldots) + \varepsilon^2\vartheta_2(T_0, T_1, T_2, \ldots) + \cdots \tag{30}$$

For convenience, let

$$\frac{\partial}{\partial T_0} = D_0, \qquad \frac{\partial}{\partial T_1} = D_1, \qquad \frac{\partial}{\partial T_2} = D_2, \ldots, \frac{\partial}{\partial T_i} = D_i, \ldots \tag{31}$$

By carrying out the expansion to the order of ε^2 and equating the coefficients of equal powers of ε, one may find the following equations:

$$D_0^2\vartheta_0 + \delta\vartheta_0 = 0 \tag{32}$$

$$D_0^2\vartheta_1 + \delta\vartheta_1 = -2D_0D_1\vartheta_0 - 2\alpha_1\vartheta_0 \cos 2T_0 - 2\alpha_2\vartheta_0 \sin 2T_0 + k_1 \cos 2T_0 + k_2 \sin 2T_0 \tag{33}$$

$$D_0^2\vartheta_2 + \delta\vartheta_2 = -2D_0D_2\vartheta_0 - D_1^2\vartheta_0 - 2D_0D_1\vartheta_1 - 2\alpha_1\vartheta_1 \cos 2T_0 - 2\alpha_2\vartheta_1 \sin 2T_0 \tag{34}$$

The general solution to Eq. (32) can be written in the form

$$\vartheta_0 = A(T_1, T_2)e^{i\beta T_0} + \bar{A}(T_1, T_2)e^{-i\beta T_0} \tag{35}$$

where $\beta = \delta^{1/2}$ and $\bar{A}$ is the complex conjugate (CC) of A. Then, Eq. (33) may be written as

$$D_0^2\vartheta_1 + \beta^2\vartheta_1 = -2i\beta D_1 A e^{i\beta T_0} - (\alpha_1 - i\alpha_2)Ae^{i(2+\beta)T_0} - (\alpha_1 - i\alpha_2)\bar{A}e^{i(2-\beta)T_0} + \tfrac{1}{2}(k_1 - ik_2)e^{i2T_0} + \mathrm{CC} \tag{36}$$

Because the behavior of the motion near resonance is of concern, a detuning parameter σ can be introduced such that

$$\beta_e = \beta + \varepsilon\sigma \tag{37}$$

where β_e is the excitation frequency. The parameter σ allows one to describe the nearness of the excitation frequency to the system frequency and helps one recognize the terms in the governing equation for ϑ_1 that lead to secular or nearly secular terms. By analyzing the particular solution of Eq. (36), one may find many resonance conditions, for example, $\beta = , \ldots, 4, 2, 1, \frac{1}{2}, \frac{1}{4}, \ldots, 0$, but here we will consider only two cases: $\beta = 2$ and $\beta = 1$.

Case $\beta \approx 2$

This is the case of combined primary resonance, that is, when the frequency of the excitation is the same as the natural frequency of the system. Because $2 = \beta + \varepsilon\sigma$, eliminating the secular terms from Eq. (36) gives

$$D_1 A = -(1/4\beta)\,(k_2 + ik_1)\,e^{i\sigma T_1} \tag{38}$$

The solutions for A and $\bar{A}$ are

$$A = A_0 - (1/4\sigma\beta)\,(k_1 - ik_2)\,e^{i\sigma T_1}$$

$$\bar{A} = \bar{A}_0 - (1/4\sigma\beta)\,(k_1 + ik_2)\,e^{-i\sigma T_1} \tag{39}$$

respectively, where A_0 and $\bar{A}_0$ are integration constants. From Eqs. (35) and (39), one may observe that, as σ approaches zero, the theoretical motion becomes unbounded; when σ is nonzero, but small, the motion is bounded with large amplitudes. Obviously, such resonances result from the external-type excitations. Because $\beta = \delta^{1/2} = 2\omega_0/\Omega$, we may represent the resonance condition $\beta \approx 2$ in terms of $\dot{\psi}$ and θ_s (as shown in Fig. 3).

Case $\beta \approx 1$

This is the case when the natural frequency of the system is close to one-half of the frequency of the parametric excitation. Because $1 = \beta + \varepsilon\sigma$, collection of the secular terms from Eq. (36) yields the following equation:

$$D_1 A = (1/2\beta)\,(\alpha_2 + i\alpha_1)\,\bar{A}e^{i2\sigma T_1} \tag{40}$$

Also we obtain a solution of Eq. (36),

$$\vartheta_1 = [1/4(\beta+1)]\left[(\alpha_1 - i\alpha_2)Ae^{i(2+\beta)T_0} + (\alpha_1 + i\alpha_2)\bar{A}e^{-i(2+\beta)T_0}\right] + [1/2(\beta^2 - 4)]\left[(k_1 - ik_2)e^{i2T_0} + (k_1 + i\alpha_2)e^{-i2T_0}\right] \tag{41}$$

Then, elimination of the secular terms from Eq. (34) when $\beta \approx 1$ requires that

$$2\beta D_2 A - iD_1^2 A + [1/4(\beta+1)](\alpha_2 - i\alpha_1)(\alpha_1 - i\alpha_2)A = 0 \tag{42}$$

From Eq. (40), we get

$$D_1^2 A = (1/4\beta^2)\left(\alpha_1^2 + \alpha_2^2\right)A - (\sigma/\beta)(\alpha_1 - i\alpha_2)\bar{A}e^{i2\sigma T_1} \tag{43}$$

Substitution of Eq. (43) into Eq. (42) gives

$$2\beta D_2 A - i\frac{\beta^2 + \beta + 1}{4\beta^2(\beta+1)}\left(\alpha_1^2 + \alpha_2^2\right)A + \frac{\sigma}{\beta}(\alpha_2 + i\alpha_1)\bar{A}e^{i2\sigma T_1} = 0 \tag{44}$$

It can be easily shown that Eqs. (40) and (44) result from a multiple-scales expansion of

$$2\beta\frac{\mathrm{d}A}{\mathrm{d}t} - i\varepsilon^2\frac{\beta^2 + \beta + 1}{4\beta^2(\beta+1)}\left(\alpha_1^2 + \alpha_2^2\right)A - \varepsilon\left(1 - \frac{\varepsilon\sigma}{\beta}\right) \times (\alpha_2 + i\alpha_1)\bar{A}e^{i2\varepsilon\sigma T_t} = 0 \tag{45}$$

Assuming a solution for Eq. (45) in the form of $A = (A_r + iA_i)e^{i\varepsilon\sigma t}$ with real A_r and imaginary A_i, we obtain

$$2\beta\frac{\mathrm{d}A_r}{\mathrm{d}t} - \left[2\varepsilon\sigma\beta + \varepsilon\left(1 - \frac{\varepsilon\sigma}{\beta}\right)\alpha_1 - \varepsilon^2\frac{(\beta^2 + \beta + 1)}{4\beta^2(\beta+1)}\left(\alpha_1^2 + \alpha_2^2\right)\right] \times A_i - \varepsilon\left(1 - \frac{\varepsilon\sigma}{\beta}\right)\alpha_2 A_r = 0 \tag{46}$$

$$2\beta\frac{\mathrm{d}A_i}{\mathrm{d}t} + \left[2\varepsilon\sigma\beta - \varepsilon\left(1 - \frac{\varepsilon\sigma}{\beta}\right)\alpha_1 - \varepsilon^2\frac{(\beta^2 + \beta + 1)}{4\beta^2(\beta+1)}\left(\alpha_1^2 + \alpha_2^2\right)\right] \times A_r + \varepsilon\left(1 - \frac{\varepsilon\sigma}{\beta}\right)\alpha_2 A_i = 0 \tag{47}$$

Equations (46) and (47) admit a solution in the form of $(A_r, A_i) = (a_r, a_i)e^{\gamma t}$ with constant a_r and a_i provided that

$$4\beta\gamma^2 = \varepsilon^2\left[\left(1 - \frac{\varepsilon\sigma}{\beta}\right)\alpha + 2\sigma\beta - \varepsilon\frac{(\beta^2 + \beta + 1)}{4\beta^2(\beta+1)}\alpha^2\right] \times \left[\left(1 - \frac{\varepsilon\sigma}{\beta}\right)\alpha - 2\sigma\beta + \varepsilon\frac{(\beta^2 + \beta + 1)}{4\beta^2(\beta+1)}\alpha^2\right] \tag{48}$$

where $\alpha = \sqrt{(\alpha_1^2 + \alpha_2^2)}$. The stability of the motion depends on the value of γ. A criterion for stability can be determined by Eq. (48). Obviously, when γ^2 is positive definite, the motion of the pendulum becomes unstable. That is, instability of the system occurs when

$$\frac{-4\beta^3 - (4-\varepsilon\alpha)\beta^2 + \varepsilon\alpha(\beta+1)}{8\beta^3(\beta+1)(1-\varepsilon\alpha/2\beta^2)}\alpha < \sigma < \frac{4\beta^3 + (4+\varepsilon\alpha)\beta^2 + \varepsilon\alpha(\beta+1)}{8\beta^3(\beta+1)(1+\varepsilon\alpha/2\beta^2)}\alpha \tag{49}$$

Because $\beta = 1 - \varepsilon\sigma$, the transition curves emanating from $\delta \approx 1$ corresponding to

$$\sigma = \pm\tfrac{1}{2}\alpha - \tfrac{1}{16}\varepsilon\alpha^2 \pm \tfrac{1}{32}\varepsilon^2\alpha^3 + \mathcal{O}(\varepsilon^3) \tag{50}$$

$$\delta = 1 \mp \varepsilon\alpha + \tfrac{3}{8}\varepsilon^2\alpha^2 \mp \tfrac{1}{8}\varepsilon^3\alpha^3 + \mathcal{O}(\varepsilon^4) \tag{51}$$

IV. Numerical Examples and Discussion

To observe the behavior of the pendulum and spacecraft motion at the QSPs during the thrusting phase, numerical simulations were conducted for the spacecraft with a configuration as given in Table 1.

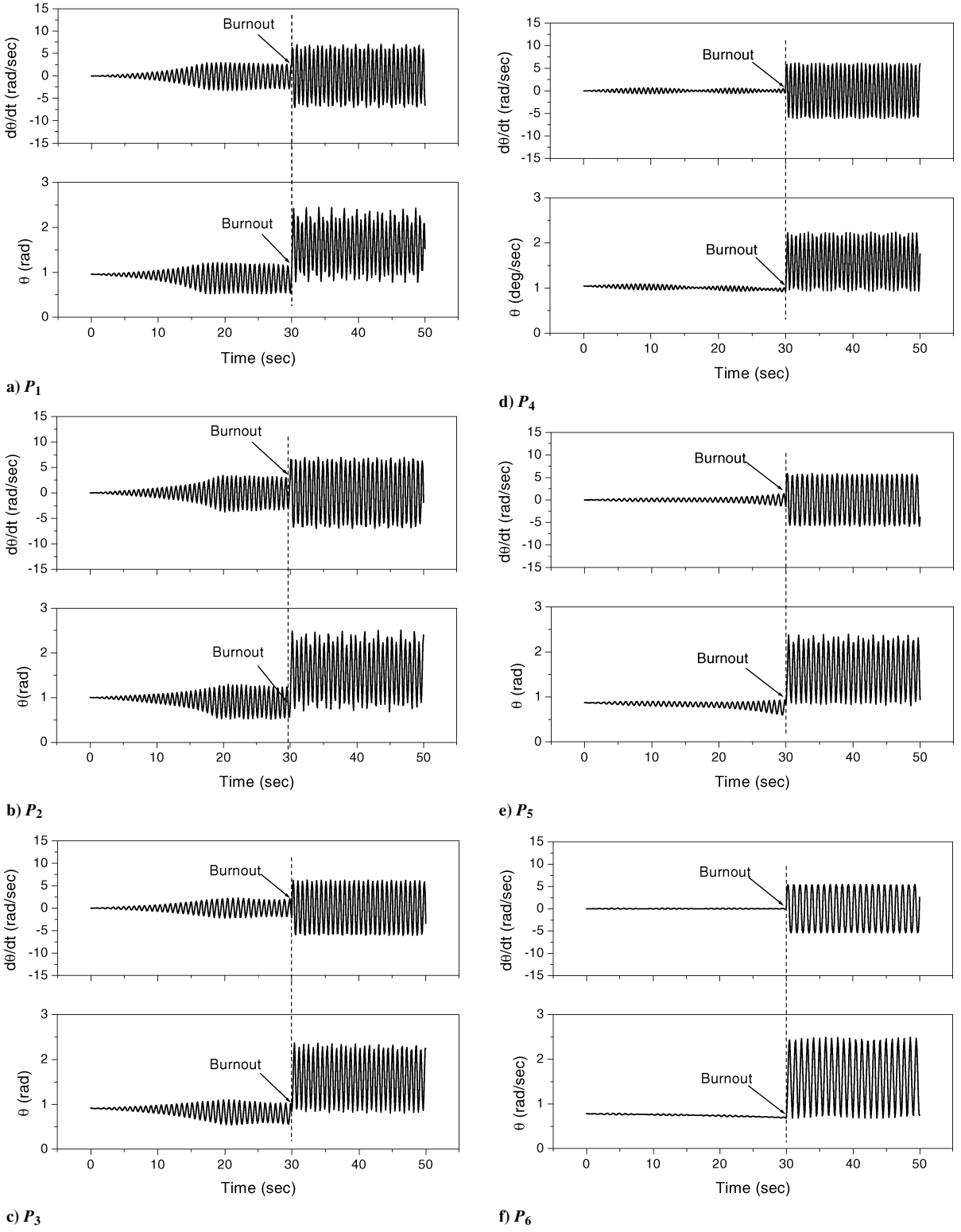

Fig. 4 Time histories of θ at unstable and stable QSPs.

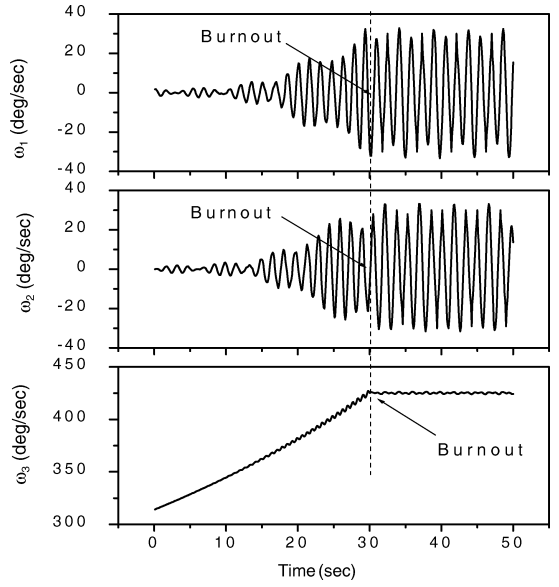

a) P_1

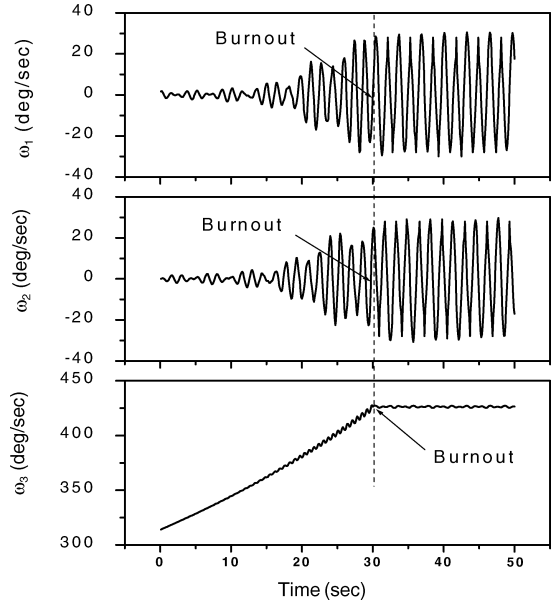

b) P_2

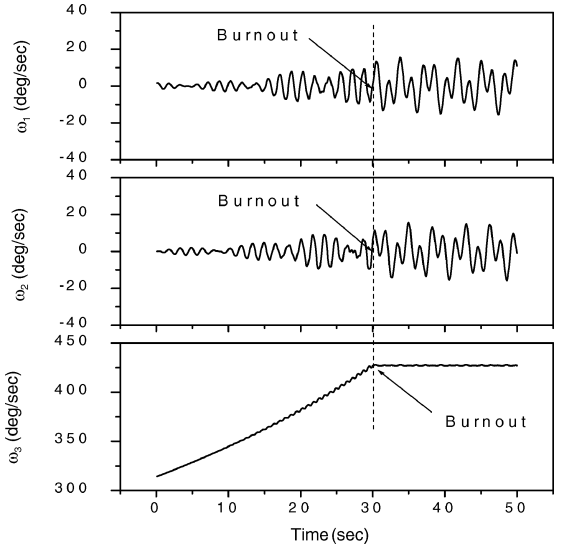

c) P_3

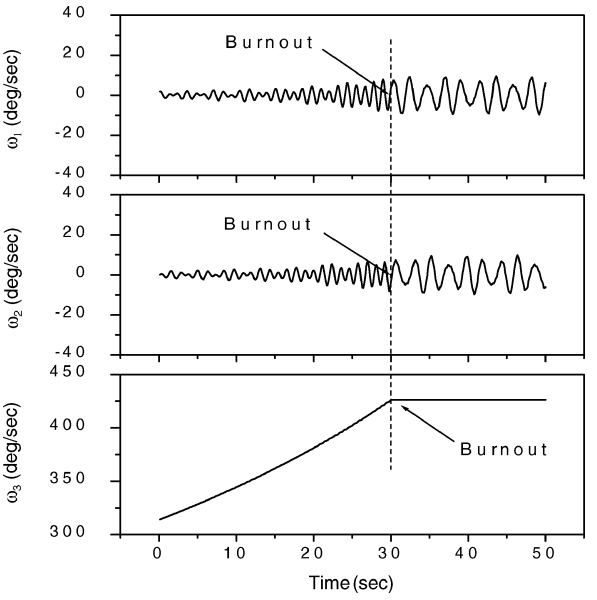

d) P_4

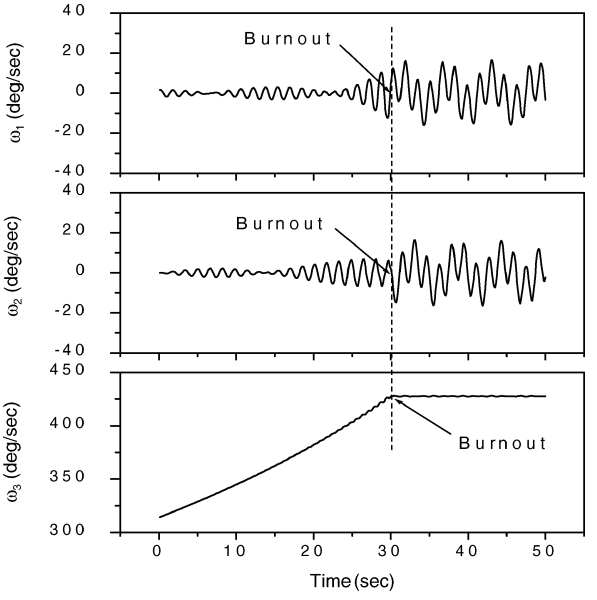

e) P_5

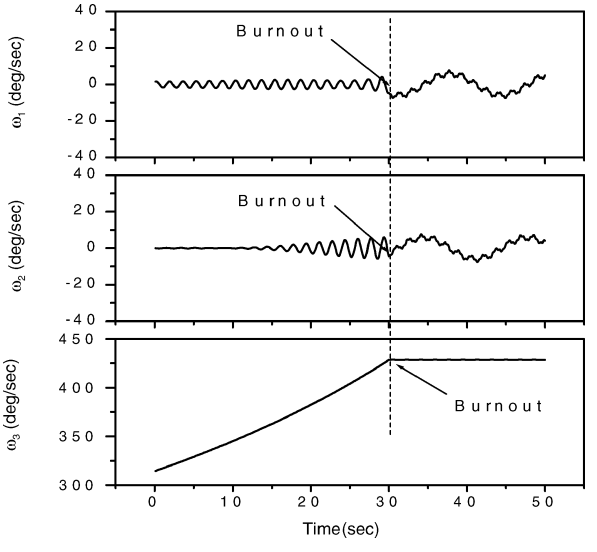

f) P_6

Fig. 5 Time histories of pitch, yaw, and roll rates at unstable and stable QSPs.

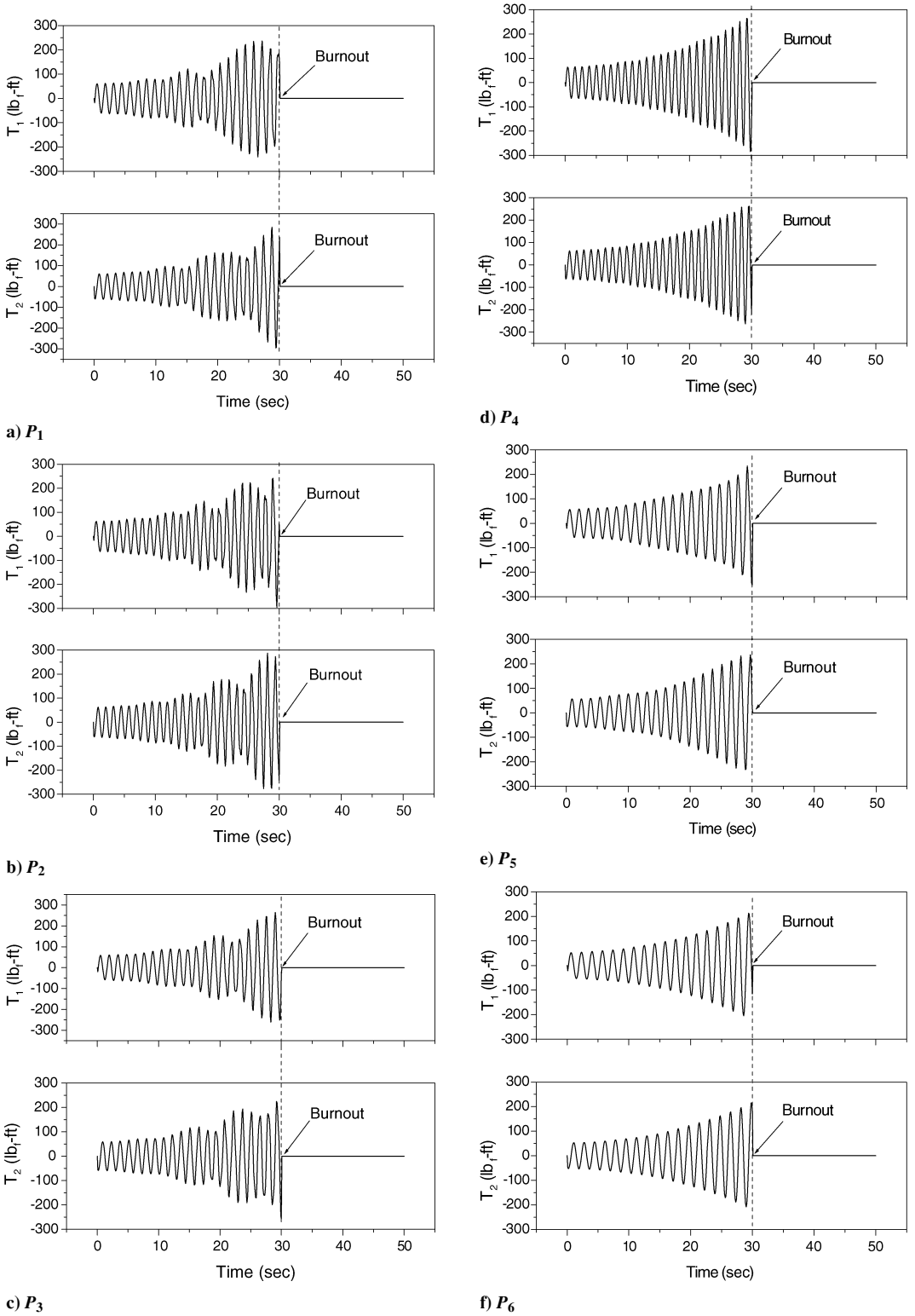

Fig. 6 Time histories of torques about the transverse axes at unstable and stable QSPs.

For convenience, we scaled down the burnout time to 30 s, and hence, the system parameters are varied with the compatible time rate. As results of simulations, we found that only the condition for $\beta \approx 2$ develops the resonant motion for the given spacecraft model and that the corresponding QSP is $\theta_s = 55$ deg. The trajectories of QSP and resonance conditions are in Fig. 3, where P_1 is a QSP satisfying the resonance condition for $\beta \approx 2$. We also examined responses of the system in the vicinity of P_1 and determined the range of θ_s that attracts the attitude motion into a resonance domain. The corresponding QSPs range from 50.40 to 58.43 deg in θ_s and 4.2 to 5.2 rad/s in $\dot{\psi}$, where the pitch and yaw rates grow as much as 17–35 deg. QSPs chosen to explain the time responses are as given in Table 2.

Figure 4a shows the time history of θ at P_1, where it has an oscillatory growth during the first half of the thrusting phase and then stabilizes during the second half. Then, immediately after burnout, the pendulum moves to a new position ($\theta = \pi/2$) and oscillates with large but bounded amplitude about that position. Figures 4b–4f show time histories of θ at QSPs other than P_1. As can be observed from Figs. 4b–4f, the responses are unstable when the QSPs are in the vicinity of P_1 and stable when the QSPs are far from P_1.

Table 2 Quasi-stationary points for numerical simulations

QSPs	P_6	P_5	P_3	P_1	P_2	P_4
θ_s, deg	45	50	52.5	55	57.5	60
$\dot{\psi}$, rad/s	3.71	4.16	4.42	4.72	5.06	5.45

Figure 5a shows the time histories of the pitch, yaw, and roll rates of the main body at P_1. Except for time length, they look similar to the observed flight telemetry as shown in Fig. 1. Figures 5b–5f show the time histories of the pitch, yaw, and roll rates at the QSPs P_2–P_6, respectively. Even though P_2 and P_3 deviate from the resonant point P_1, the responses are still unstable. We may interpret this as a characteristic of the response of the nonsationary system. Theoretically, in the stationary system, resonance domains are disjunct and one resonance condition exists for a particular configuration of the system. However, if the frequency of the excitation is time dependent, that is, nonstationary, the deviation of the response may occur near the resonance condition. The pitch, yaw, and roll rates at P_4–P_6 have small but irregular amplitudes when compared with those of the unstable QSPs.

Figures 6a–6f show the time histories of the disturbance torques about the transverse axes of the main body, which result from deviation of the center of mass from the line of thrust vector. During motor burn, pitch and yaw torques grow at the same rate with a 90-deg phase difference and drop to zero at burnout. It is evident that during the thrusting phase the motion of the pendulum significantly affects the attitude motion of the spacecraft.

At P_1, during motor burn, the pitch and yaw rates (0.65 Hz) of the main body oscillate in tune with approximately one-half of the pendulum frequency (approximately 1.30 Hz), but out of tune with the frequencies of the disturbance torques (0.75 Hz). After burnout, the frequencies of the pitch and yaw rates are the same as before, whereas the pendulum frequency increases to 1.6 Hz. Of course, after burnout the spacecraft is in thrust-free motion and the disturbance torques about the pitch and yaw axes disappear. At stable QSPs (P_4–P_6), the pitch, yaw, and roll rates oscillate almost in tune with the frequencies of the corresponding disturbance torques.

V. Conclusions

By assuming that both the main body (spacecraft) and the pendulum (slag pool) were in states of steady spin about the symmetry axis of the spacecraft, and using the multiple scale method, we obtained a quasi-stationary solution and two approximate resonance conditions of the pendulum motion. The first case of resonant motion ($\beta \approx 2$) occurs when the natural frequency of the pendulum approaches to one-half of the frequency of the parametric excitation by the main body, and the second case ($\beta \approx 1$) occurs when the frequency of the external-type excitation by the main body is close to the natural frequency of the pendulum. However, as results of numerical simulations, we found that only the parametric excitation develops the resonant motion for the given spacecraft model, and when this condition and exact full nonlinear equations are used, the responses show quite similar characteristics of the coning motion as observed.

The following is a summary of the study:

1) Motion of the pool of accumulated slag may be influenced by parametric and external-type excitations caused by the main body. However, the instability of the attitude motion as observed in PAM-D type spacecraft can be developed by only parametric excitation. At or near the QSP of P_1 that satisfies this type of resonance condition, the responses are attracted to a limit cycle.

2) During the thrusting phase, by interacting with the main body motion, the pool serves as an energy storage and generates disturbance torques about the pitch and yaw axes.

3) Because the disturbance torques are oscillatory divergent, they do not always cause attitude instability. If the frequencies of torques approach exactly or closely to those of pitch and yaw rates, the attitude motion is stable, and if not, the transverse angular momentum builds up, and hence, the attitude motion becomes unstable.

4) The practical importance of the work was to present a model that overcomes many of the problems of previous models, which failed to predict the observed motion before and after burnout, and to determine exact resonance conditions for the attitude motion of the PAM-D spacecraft in question. Therefore, the analyses have been done for fixed parameters, that is, real flown spacecraft data rather than for a wider parameter space. However, concerning the design and manufacture of new spacecraft, it is important to do analysis for a wider parameter space. Our next work will consider this aspect and cover a wider range of parameters of the spacecraft. For this purpose, even though the second resonant condition may not be established in the given spacecraft model, stability criteria in parameter space was determined.

References

[1]Flandro, G. A., "Fluid Mechanics of Spinning Rockets," Air Force Rocket Propulsion Lab., Final Rept. AFRPL-TR-86-072, Edwards AFB, CA, Jan. 1987.

[2]Flandro, G. A., Leloudis, M., and Roach, R., "Flow Induced Nutation Instability in Spinning Solid Propellant Rockets," Astronautics Lab. (AFSC), Final Rept. AL-TR-89-084, Edwards AFB, CA, April 1990.

[3]Roach, R., Burnley, V., Flandro, G. A., and Burnette, J., "Internal Ballistics Interactions in Spinning Rocket Nutation Instability," AIAA Paper 90-0042, Jan. 1990.

[4]Cheung, H., and Cohen, N. S., "Performance of Solid Propellants Containing Metal Additives," *AIAA Journal*, Vol. 3, No. 2, 1965, pp. 250–257.

[5]Crowe, C. T., and Willoughby, P. G., "A Mechanism for Particle Growth in a Rocket Nozzle," *AIAA Journal*, Vol. 4, No. 9, 1966, pp. 1677, 1678.

[6]Crowe, C. T., and Willoughby, P. G., "A Study of Particle Growth in a Rocket Nozzle," *AIAA Journal*, Vol. 5, No. 7, 1967, pp. 1300–1304.

[7]Boraas, S., "Modeling Slag Deposition in the Space Shuttle Solid Rocket Motor," *Journal of Spacecraft and Rocket*, Vol. 21, No. 1, 1984, pp. 47–54.

[8]Haloulakas, V. E., "Slag Mass Accumulation in Spinning Solid Rocket Motors," *Journal of Propulsion*, Vol. 7, No. 1, 1991, pp. 14–21.

[9]Fredrick, R. A., Jr., Nichols, J. A., and Rogerson, J., "Slag Accumulation Measurements in a Strategic Solid Rocket Motor," AIAA Paper 1996-2783, June 1996.

[10]Abramson, N. H. (ed.), *The Dynamic Behavior of Liquids in Moving Containers with Applications to Space Vehicle Technology*, NASA SP-106, 1966, Chap. 6.

[11]Hill, D. E., "Dynamics and Control of Spin-Stabilized Spacecraft with Sloshing Fluid Stores," Ph.D. Dissertation, Dept. of Mechanical Engineering, Iowa State Univ., Ames, IA, 1985.

[12]Hill, D. E., and Baumgarten, J. R., "Dynamic Simulation of Spin-Stabilized Spacecraft with Sloshing Fluid Stores," *Journal of Guidance, Control and Dynamics*, Vol. 11, No. 6, 1988, pp. 597–599.

[13]Cochran, J. E., Jr., and Kang, J. Y., "Nonlinear Stability Analysis of the Attitude Motion of a Spin-Stabilized Upper Stage," *Advances in the Astronautical Sciences*, Vol. 75, No. 1, 1991, pp. 345–364.

[14]Or, A. C., "Rotor-Pendulum Model for the Perigee Assist Module Nutation Anomaly," *Journal of Guidance, Control, and Dynamics*, Vol. 15, No. 2, 1992, pp. 297–303.

[15]Or, A. C., and Challoner, A. D., "Stability of Spinning Spacecraft Containing Shallow Pool of Liquid Under Thrust," *Journal of Guidance, Control, and Dynamics*, Vol. 17, No. 5, 1994, pp. 1019–1027.

[16]Meyer, R. X., "Coning Instability of Spacecraft During Periods of Thrust," *Journal of Spacecraft and Rockets*, Vol. 33, No. 6, 1996, pp. 781–788.

[17]Mingori, D. L., and Yam, Y., "Nutation Instability of a Spinning Spacecraft with Internal Mass Motion and Axial Thrust," AIAA Paper 86-2271, Aug. 1986.

[18]Yam, Y., Mingori, D. L., and Halsmer, D. M., "Stability of a Spinning Axisymmetric Rocket with Dissipative Internal Mass Motion," *Journal of Guidance, Control, and Dynamics*, Vol. 20, No. 2, 1997, pp. 306–312.

[19]Hung, R. J., "Effect of the Baffle on the Spacecraft Fluid Propellant Viscous Stress and Moment Fluctuations," *Transactions of the Japan Society for Aeronautical and Space Sciences*, Vol. 36, No. 110, 1993, pp. 187–207.

[20]Cho, S., McClamroch, N. H., and Reyhanoglu, M., "Feedback Control of a Space Vehicle with Unactivated Fuel Slosh Dynamics," AIAA Paper 2000-4046, Aug. 2000.

[21]Hughes, P. C., *Spacecraft Attitude Dynamics*, Wiley, New York, 1986, pp. 97, 526.

[22]Cochran, J. E., Jr., "Nonlinear Resonances in the Attitude Motion of a Dual-Spin Spacecraft," *Journal of Spacecraft and Rockets*, Vol. 14, No. 9, 1977, pp. 562–572.

[23]Nayfeh, A. H., and Mook, D. T., *Nonlinear Oscillations*, Wiley, New York, 1979, pp. 56–59.